An application of the SCF, MBPT and CC correlated densities: a graphical display along the potential energy surface of $CH_4 \rightarrow CH_3 + H$

C. Sosa, G. W. Trucks, G. D. Purvis III and R. J. Bartlett

Quantum Theory Project, University of Florida, Gainesville, FL, USA

The potential energy surface for the dissociation of methane $CH_4 \rightarrow CH_3 + H$ is investigated by displaying the gradients of the SCF and correlated electron density as colored regions on isodensity surfaces. It is shown that coloring the gradients of the electron density is sensitive enough to show differences among the SCF, MBPT(2), D-MBPT(4) and L-CCD densities.

Keywords: methane dissociation; correlated density; electron density; graphical display; self-consistent field method (SCF); second-order many-body perturbation theory (MBPT)(2); fourth-order many-body perturbation theory with double excitations (D-MBPT)(4); linearized coupled-cluster method with double excitations (L-CCD)

The wide use of standard quantum mechanical *ab initio* programs has created the need for sophisticated graphics programs, capable of displaying the information contained in the wave function. In the past, the interpretation of *ab initio* results in terms of classical chemical concepts has been usually provided by expressing electronic populations as atomic charges or bond populations. In general, the electronic population analysis is based on the one-particle density matrix. Although it is well known that Mulliken population[1] or Löwdin population[2] are highly basis set dependent, they still provide good qualitative results when compared within a homologous series of molecules with the same basis set. However, from the viewpoint of rigor, the density is much to be preferred since, unlike a population analysis, the density is a quantum mechanical observable.

Hence, it seems more desirable to observe directly changes in the molecular electron density. The chemistry of a molecule is determined by the electron cloud surrounding the molecule. Changes in the electronic cloud along the reaction path can be used to correlate, explain and predict differences in chemical reactions, such as $CH_4 \rightarrow CH_3 + H$.[3-6] In previous work, Purvis and Culberson[7-9] have shown that coloring the density by the magnitude of the gradient provides an intrinsic mechanism for mapping the underlying atomic structure in vivid hues commonly used in molecular ball-and-stick models.

One-particle density matrices at the SCF level are routinely computed in all *ab initio* programs. In an orthonormal basis set the density is simply defined as

$$D_{\mu\nu}^{SCF} = \sum_i C_{\mu i} C_{\nu i}^*$$

where the Cs are the expansion coefficients. However, it is well documented in the literature[10] that correlation corrections are crucial in the description of potential energy surfaces. Therefore, correlated density matrices are needed for the proper representation of the molecular electron density along the reaction paths. At the correlated level, that is, within the many-body perturbation theory (MBPT) and coupled-cluster (CC) methods, energy derivative expressions allow the definition of correlated density matrices. The density matrix obtained from this approach has been referred by Salter *et al.*[11] and Trucks *et al.*[12-13] as the *response* density, since the density includes orbital relaxation.

In this work we use computer-generated graphics showing colored isodensity surfaces to study the differences of the Hartree-Fock and correlated wave functions along the reaction path. Changes in colored patterns reflect small changes in the magnitude of the electron density gradient, which are readily interpreted.

Address reprint requests to Dr. Bartlett at the Quantum Theory Project, University of Florida, Gainesville, FL 32611, USA.
Received 16 November 1988; accepted 16 November 1988

METHOD

Ab initio molecular orbital calculations are performed with the ACES system of programs.[14] A Gaussian type double-zeta plus polarization (DZP) basis consisting of (9s5p1d) Huzinaga's uncontracted[15] with Dunning's[16] (4s2p1d) contraction are used for the SCF and correlated calculations. An exponent of 0.75 is used for carbon. Electron correlation is estimated using MBPT(2), MBPT(3), and D-MBPT(4) as well as coupled-cluster (L-CCD).[17] Single point calculations of the correlated energies and densities are performed by elongating one of the C-H bonds along the z-axis and fixing the HCH angle to the values reported by Duchovic *et al.*[3]

Molecular densities are constructed at both the SCF and correlated levels. The total electron density is defined as a response property. Response properties are associated with the derivative of the energy with respect to a perturbation parameter, λ. This parameter controls the magnitude of a one-electron potential energy perturbation, $\lambda\mathcal{O}$. For example, the z-component of the dipole moment is the first-order response of the system to a uniform electric field:

$$\lambda\mathcal{O} = \lambda \sum_{i}^{e^-} z_i$$

Likewise, the perturbation may be the delta function:

$$\lambda\mathcal{O} = \lambda \sum_{i}^{e^-} \delta (r_i - r)$$

For this choice of perturbation, the energy derivative is the electron density evaluated at point r. The form of the electron density ρ is given by

$$\rho(r) = \sum_{\mu,\nu} \mathcal{D}_{\mu\nu}^{total} \chi_\mu^* (r) \chi_\nu (r)$$

where χ denotes the atomic orbital basis set and $\mathcal{D}^{\text{total}}$ is the total density matrix defined by adding the correlated contribution to the SCF density matrix or

$$\mathcal{D}_{\mu\nu}^{total} = D_{\mu\nu}^{SCF} + D_{\mu\nu}^{Corr}$$

The explicit form of the total density matrix, as well as a complete derivation, is given elsewhere.[11-13]

The three-dimensional (3D) isodensity surfaces are displayed using ELESTA, C3D, and CMOL computer programs designed for a Silicon Graphics Iris 3030 with a resolution of 768 × 1024 × 32 bitplanes, 8 MB of main memory, hardware floating point, FORTRAN compiler, GL2, UNIX 5.3, hardware Zbuffer option and 19 inch monitor. The CMOL program requires that MEX (multiple exposure window manager) be running.

ELESTA calculates molecular electrostatic potentials and molecular electronic densities and gradients of the density on a 3D grid of points. Execution time for each of the points for CH_4 took around 45 minutes of CPU time on the Iris. The input for ELESTA corresponds to the SCF or correlated densities computed using the ACES system of programs. The SCF and correlated densities were generated on the CRAY XMP/48 at the Pittsburgh Supercomputing Center. Each point at the SCF level takes around 45 seconds of CPU time. The execution time for each correlated calculation varies from about 60 seconds to less than 500 seconds of CPU time. C3D reads the files produced by ELESTA, finds constant valued surfaces at specified function values and writes a triangle file defining the constant valued surfaces and contains the Cartesian coordinates, the gradient directions, and a function value for each corner of each triangle. CMOL reads the triangle file, the molecular conformation file, the light direction file and the color definition file. Then it displays the constant value surfaces and molecular framework and permits the user to manipulate the displayed surfaces interactively.

GRAPHICAL REPRESENTATION

The molecular electron density, $\rho(r;R)$, constitutes a scalar field defined over all space, r, and all nuclear arrangements, R. Thus, the density can have gradients $\nabla\rho(r)$, and with respect to internuclear arrangements, R, $\nabla\rho(R)$. For the density, $\nabla\rho(r)$ represents the neighboring anisotropy of the density. The shortest path between two bonded nuclei that passes through the saddle point of the electronic density in the internuclear region and follows the density gradient from the saddle point to each nucleus is the bond path, defined by Bader.[18] Concepts such as partitioning surfaces and atoms in a molecule are also derived from $\nabla\rho(r)$. For both ρ, the gradient with respect to r can be useful in generating effective graphical displays.

The gradient of the density on an isodensity surface is a vector field perpendicular to the isodensity surface. Therefore, a two-dimensional drawing of an isodensity surface, which uses shading to represent curvature in the third dimension, also fully encodes the directional dependence of the gradient. The magnitude of the gradient can be added to the isodensity by coloring the surface. Thus, an isodensity surface, colored with the magnitude of the gradient, provides a simultaneous representation of both the density and the gradient of the density. The implementation of the algorithm has been described elsewhere.[7-9]

RESULTS AND DISCUSSION

The calculations are performed as described in more detail elsewhere.[6] Figure 1 shows the geometry used throughout the calculations. Table 1 summarizes all the parameters used for each of the points along the reaction path. For C-H bond lengths between 0.75-1.5 Å, calculations have been carried out using RHF. For bond lengths greater than 1.5Å, RHF and UHF calculations were performed for each of the points. The characteristic features of the Hartree-Fock approximation to a potential energy surface for single bond breakings are well documented in the literature.[19-22] The RHF exhibits a correct qualitative behavior at the equilibrium geometry; however, it is well known that at infinite separation the RHF goes to the wrong energy limit and, consequently, the wave function incorrectly describes the

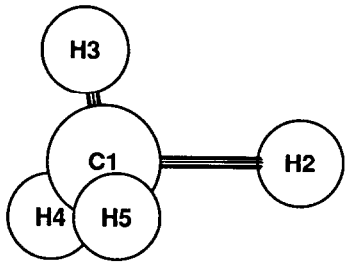

Figure 1. Geometry of the CH_4 system throughout the reaction. The C_1–H_2 bond is being elongated along the z-axis

Table 1. Bond lengths and angles used along the potential energy surface

Bond length (Å)	Angle (degrees)
0.757	111.08
1.086	109.47
1.500	105.89
2.000	100.57
2.500	96.29
3.000	91.95
∞	90.00

Note: All parameters were obtained from Ref. 3

CH_3 + H electronic state. On the other hand, the UHF provides an alternative solution to the dissociation problem, that is, the wave function gives a qualitatively correct description of the CH_3 + H fragments at infinite separation. At about 1.5Å, the E_{UHF} becomes different from the E_{RHF}; at this point the convergence as well as the density matrix between the RHF and the UHF are quite different. This can be easily observed by looking at the charge distribution based on a Mulliken population analysis, which indicates that the hydrogen participating in the bond breaking is negatively charged in the RHF wave function, while it is neutral in the UHF case.

The information stored in the wave function can be vividly displayed as isodensity surfaces colored by the magnitude of the gradient. This colored representation provides a qualitative description of the electronic response to structural perturbations under certain types of constraints, such as the RHF. The sensitivity of this method is illustrated in Color Plate 1, which shows the 0.05 isodensity* surface of CH_3 + H computed at the RHF (R = 2.0, 2.5, and 3.0 Å) and UHF (R = 2.0 Å) levels, respectively. The color coding used for the magnitude of the gradients is shown as a table in the upper left corner in each of the figures. Clearly, the most noticeable difference is the color of the gradient on the hydrogen atom involved in the C-H bond breaking. In the RHF case (Color Plate 1a–c) the magnitude of the gradient is smaller than the UHF (Color Plate 1d). This indicates that as the C-H bond begins to break, the RHF wave function builds up density on the H atom faster than the UHF, forming $CH_3^{\delta+}$ and $H^{\delta-}$.

Table 2 summarizes the correlated energies. Comparing the MBPT(4) energies based on RHF and UHF reference functions, the following well-known facts [3-6,17,21,22,23] can be summarized:

1. The RMBPT(n); n = 2,3,4 curves go to the wrong energy limit
2. Triple excitations are very important in the 2.0–3.0 Å range for the UMBPT(4) calculations
3. Single excitations are almost as important as triple excitations for the RMBPT(4) calculations
4. RMBPT(n) breaks down at large internuclear distances
5. UMBPT(4) calculations suffer from spin contamination
6. CCSD methods introduce single excitations and lower the potential energy curve compared to CCD
7. CCSDT-1 introduces the effect of linear triples. Using an RHF reference, this model recovers most of the correlation effects obtained from MR-CI. Using a UHF reference, it also recovers most of the correlation effects, but some spin contamination remains in the wave function
8. The full CCSDT and its approximations CCSDT-n; n = 2–4, recover all the correlation effects obtained from MR-CI calculations

From Figure 2 some of these results may be observed. The RMBPT(2) goes to the wrong energy limit, while the UMBPT(2) gives a qualitatively correct description of the C-H bond breaking, but suffers from spin contamination; D-RMBPT(4) improves the agreement but still breaks down at large internuclear distances. On the other hand, it is interesting to note that L-RCCD diverges quicker than the MBPT(n) series. As mentioned above this is well documented in the literature.[21]

However, there are some features that may be discussed in terms of the gradients of the electron density. Color Plate 2 represents the 0.05 isodensity surfaces of the $CH_4 \rightarrow CH_3$ + H bond breaking. Each frame corresponds to a point along the reaction path computed at the D-MBPT(4) level. A simple perturbational molecular orbital (PMO) model can be constructed to explain the trends of the gradients along the potential energy surface at the SCF level. The main orbitals involved in this reaction are the σ_{C-H} and σ^*_{C-H} of methane. These sigma-type bonds correspond to the C-H bond that is being elongated. For R = 0.757, 1.086, and 1.5 Å, the potential energy surface is equally well described with RHF or UHF wave functions. Hence, most of the changes in the gradients of the density are due to the fact that the C-H bond has been elongated and the C-H electron density decreases from the center of the bond toward the sides (Color Plate 2a–c). However, as the C-H bond is stretched beyond 1.5 Å the RHF and UHF methods diverge. As the reaction progresses, the orbital interac-

*This isodensity definition has been taken from Ref. 9. The term 0.05 isodensity means the orbital density on this surface has a value of 0.05. Since there are two electrons for orbital in CH_4, the electron density in the 0.05 isodensity surface is 0.10.

Table 2. Correlation energies of CH_4 along the potential energy surface

R	Method	SCF	MBPT(2)	D-MBPT(4)	L-CCD
0.757	RHF	−40.062432	−40.236096	−40.260328	−40.262214
1.086	RHF	−40.207590	−40.382830	−40.407502	−40.409701
1.500	RHF	−40.149936	−40.327484	−40.354028	−40.357799
2.000	RHF	−40.059940	−40.242898	−40.275730	−40.286141
	UHF	−40.084361	−40.234890	−40.259850	
2.500	RHF	−39.993005	−40.186771	−40.230710	−40.258473
	UHF	−40.072233	−40.215145	−40.238485	
3.000	RHF	−39.944733	−40.156364	−40.216985	−40.282670
	UHF	−40.070057	−40.211573	−40.234785	
CH_3 + H	UHF	−40.069281	−40.210319	−40.233521	−40.235759
ΔE^a		86.8	108.3	109.2	109.2

Note: Energies in au
[a] $\Delta E = E(CH_3 + H) - E(R = 1.086)$ in kcal/mol

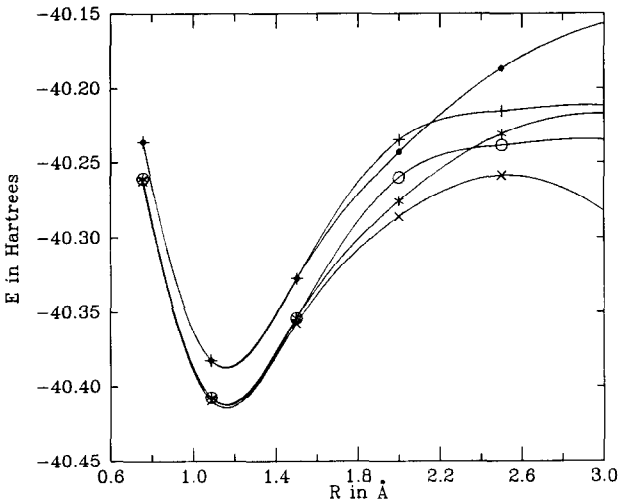

*Figure 2. Potential energy curves for $CH_4 \rightarrow CH_3 + H$. ● RMBPT(2), + UMBPT(2), * D-RMBPT(4), ○ D-UMBPT(4), x L-CCD*

tion decreases, that is, the gap between the HOMO-LUMO becomes smaller. At R = 2.0 Å the RHF is no longer a good reference function, since two electrons have to remain paired. For R = 2.5 Å the HOMO-LUMO gap is smaller and the σ^*_{C-H} has to be populated due to the RHF constraint. Hence, the gray color of the hydrogen atom at the SCF level (Color Plate 1c). However, a different picture emerges at the correlated level. When the CH_3 + H are at a distance of R = 3.0 Å apart, the two fragments are almost completely dissociated. Color Plates 2f and 2g show the RMBPT(4) and UMBPT(4) densities. The RMBPT(4) frame is characterized by a hydrogen with a large gradient. The UMBPT(4) frame has a hydrogen with a smaller gradient. The magnitudes of the gradients for the UMBPT(4) and UHF densities appear to be in good agreement. On the other hand, the magnitudes of the gradients at RMBPT(4) level appear to indicate that the electronic charge is being displaced toward the CH_3 group. Hence, the blue color on the hydrogen at R = 3.0 Å (Color Plate 2f).

It is also interesting to compare changes in the correlated densities (Color Plates 2d-f and 3a-c). Color Plates 2d and 3a correspond to R = 2.0 Å and D-MBPT(4) and L-CCD correlated densities. Both isodensity surfaces are very similar. This is not surprising, since the behavior of the wave functions as well as the total energies (see Figure 2) at this internuclear distance are in good agreement. However, as the C-H bond length is elongated more than two times its equilibrium distance, a difference between the two isodensities can be observed. Color Plates 2e and 3b correspond to the D-MBPT(4) and L-CCD 0.05 isodensity surfaces. As the H atom moves away from the $-CH_3$ fragment, the gradient on the hydrogen surface increases rapidly. At this point two factors are contributing to the rapid change in the gradient: (1) the RHF wave function has become a poor reference function, and (2) higher-order corrections are needed to overcome the RHF deficiencies. In both bases, that is, D-MBPT(4) and L-CCD methods, higher order corrections are not introduced, and at R = 3.0 Å both models give a poor description of the $CH_4 \rightarrow CH_3$ + H dissociation. At R = 3.0 Å L-CCD diverges more rapidly. Correlated densities computed with CCSDT-n methods based on RHF reference functions are expected to provide a better description of the charge distribution.[6] Currently we are in the process of generating higher order correlated densities.

CONCLUSIONS

Gradients of the SCF and correlated densities displayed as colored isodensity surfaces are shown to be sensitive enough to provide insights on the quality of the wave function. Furthermore, the method has proven to be able to distinguish between RHF and UHF wave functions. It has also indicated that the behavior of the wave function at the SCF level cannot be extrapolated to the correlated results in some cases.

ACKNOWLEDGEMENT

This research was supported by AFOSR. The calculations of the energies and correlated densities were performed at the Pittsburgh Supercomputing Center with a computational grant from the National Science Foundation.

REFERENCES

1 Mulliken, R. S. *J. Chem. Phys.* 1955, **23,** 1833
2 Löwdin, P. O. *Phys. Rev.* 1955, **97,** 1474
3 Duchovic, R. J., Hase, W. L., Schlegel, H. B., Frisch, M. J. and Raghavachari, K. *Chem. Phys. Lett.* 1982, **89,** 120
4 Brown, F. B. and Truhlar, D. G. *Chem. Phys. Lett.* 1985, **113,** 441
5 Hirst, D. M. *Chem. Phys. Lett.* 1985, **122,** 225
6 Sosa, C., Noga, J., Purvis, G. D. and Bartlett, R. J. *Chem. Phys. Lett.* 1988, **153**, 139
7 Purvis, G. D. and Culberson, C. *Geometrical Derivatives of Energy Surfaces and Molecular Properties* (Jorgensen, P. and Simons, J., Eds.) Reidel Publishing Co., Dordrecht, 1986
8 Purvis, G. D. and Culberson, C. *Int. J. Quantum* Chem. 1986, **S13**, 261
9 Purvis, G. D. and Culberson, C. *J. Mol. Graphics* 1986, **4,** 88
10 Bartlett, R. J. *Annu. Rev. Phys. Chem.* 1981, **32,** 359
11 Salter, E. A., Trucks, G. W., Fitzgerald, G. and Bartlett, R. J. *Chem. Phys. Lett.* 1987, **141**, 61
12 Trucks, G. W., Salter, E. A., Sosa, C. and Bartlett, R. J. *Chem. Phys. Lett.* 1988, **147,** 359
13 Trucks, G. W., Salter, E. A., Noga, J. and Bartlett, R. J. *Chem. Phys. Lett.* 1988, **150**, 37
14 *ACES* (Advanced Concepts in Electronic Structure) —an *ab initio* program system, authored by Bartlett, R. J., Purvis, G. D., Fitzgerald, G. B., Harrison, R. J., Lee, Y. S., Laidig, W. D., Cole, S. J., Magers, D. H., Salter, E. A., Trucks, G. W., Sosa, C., Rittby, M. and Pal, S. Quantum Theory Project, University of Florida, Gaincsville, FL, 1987. The CRAY version of the *ACES* system of programs is available from R. J. Bartlett at the Quantum Theory Project
15 Huzinaga, S. *J. Chem. Phys.* 1965, **42**, 1293
16 Dunning, T. H. *Chem. Phys.* 1970, **53,** 2823
17 Bartlett, R. J. and Purvis, G. D. *Int. J. Quantum Chem.* 1978, **14,** 561
18 Bader, R. F., Tang, T.-H., Tal, Y. and Biegler-Konig, F. W. *J. Am. Chem. Soc.* 1982, **104**, 940
19 Mayer, I. *Int. J. Quantum Chem.* 1978, **14,** 29
20 Klimo, W. and Tino, J. *Int. J. Quantum Chem.* 1984, **15**, 733
21 Bartlett, R. J. and Purvis, G. D. *Physica Scripta* 1980, **21,** 255
22 Laidig, W. L., Saxe, P. and Bartlett, R. J. *J. Chem. Phys.* 1987, **86,** 887
23 Schlegel, H. B. *J. Chem. Phys.* 1986, **84,** 4530